AIP Journal of Applied Physics

High near-infrared transparency and carrier mobility of Mo doped In 2 O 3 thin films for optoelectronics applications

S. Parthiban, E. Elangovan, K. Ramamurthi, R. Martins, and E. Fortunato

Citation: Journal of Applied Physics **106**, 063716 (2009); doi: 10.1063/1.3224946
View online: http://dx.doi.org/10.1063/1.3224946
View Table of Contents: http://scitation.aip.org/content/aip/journal/jap/106/6?ver=pdfcov
Published by the AIP Publishing

High near-infrared transparency and carrier mobility of Mo doped In_2O_3 thin films for optoelectronics applications

S. Parthiban,[1] E. Elangovan,[2] K. Ramamurthi,[1,a)] R. Martins,[2] and E. Fortunato[2]
[1]*Crystal Growth and Thin Film Laboratory, School of Physics, Bharathidasan University, Tiruchirappalli-620 024, India*
[2]*CENIMAT-I3N and CEMOP-UNINOVA, Materials Science Department, FCT-UNL, 2829-516 Caparica, Portugal*

(Received 6 July 2009; accepted 12 August 2009; published online 25 September 2009)

Molybdenum (0–1 at. %) doped indium oxide thin films with high near-infrared (NIR) transparency and high carrier mobility were deposited on Corning-1737 glass substrates at 400 °C by a spray pyrolysis experimental technique. X-ray diffraction (XRD) analysis confirmed the cubic bixbyite structure of indium oxide. The preferred growth orientation along the (222) plane for the low Mo doping level (≤0.5 at. %) shifts to (400) for higher Mo doping levels (>0.6 at. %). The crystallite size extracted from the XRD data corroborates the changes in full width at half maximum due to the variation in Mo doping. A scanning electron microscopy study illustrated the evolution in the surface microstructure as a function of Mo doping. The negative sign of the Hall coefficient confirmed the *n*-type conductivity. A high carrier mobility of ~122.4 $cm^2/V\,s$, a carrier concentration of $\sim 9.5\times 10^{19}$ cm^{-3}, a resistivity of $\sim 5.3\times 10^{-4}$ Ω cm, and a high figure of merit of $\sim 4.2\times 10^{-2}$ Ω^{-1} are observed for the films deposited with 0.5 at. % Mo. The obtained high average transparency of ~83% in the wavelengths ranging from 400 to 2500 nm confirmed the extension of transmittance well into the NIR region. © *2009 American Institute of Physics*. [doi:10.1063/1.3224946]

I. INTRODUCTION

Transparent conducting oxide (TCO) thin films with a unique combination of low resistivity (ρ), high carrier mobility (μ), and near-infrared (NIR) transmittance are desired for optoelectronics applications.[1] Transparent thin film transistors require high channel mobility to improve device performance, and solar cells require high NIR transparency to widen the spectral sensitivity in the entire visible-NIR region.[2–4] Numerical simulation using the Drude model authenticates that the higher NIR transparency (T) can be achieved by increasing the μ of TCO films.[5] A number of TCOs, including zinc oxide (ZnO), indium oxide (In_2O_3), and tin oxide (SnO_2), are known to exist for many years. However, commercial TCOs (SnO_2:In, SnO_2:F, and ZnO:Al) suffer from free-carrier absorption in the NIR region and hence limit μ.[6] Photovoltaic industry demands TCOs to transmit the entire solar spectrum for electrode applications. The short-wavelength [ultraviolet (UV)] cutoff corresponds to the fundamental band gap energy of the materials, whereas the long-wavelength [infrared (IR)] edge corresponds to the free-carrier plasma resonance frequency. These critical optical properties are directly influenced by the carrier concentration (n) and μ, as has been explained for tin doped indium oxide (ITO) by Frank and Kostlin.[7] In general, for a material to be transparent across the visible spectrum, its band gap must be greater than 3 eV to enable transmission up to the near UV (400 nm) wavelength, and its free-carrier plasma resonance frequency absorption must lie in the NIR (1500 nm) or IR. Increasing n decreases ρ but also has the drawback of shifting the IR absorption edge toward the visible region, thus narrowing the window. This phenomenon is determined by the plasma oscillation of the free carriers that screen incident electromagnetic wave via intraband transitions within the conduction band. The IR reflection in ITO is well predicted by the Drude model.[5] The position of the UV edge depends, in part, on the n in the material. A straightforward analysis of the density of states in the conduction band reveals that the UV edge will shift to shorter wavelengths with increasing n because the change in the optical band gap (ΔE) increases the carrier density[8] as $\Delta E \sim n^{3/2}$.

However, the use of high μ and NIR transparent conductors has been limited in the electronic device applications owing to the limited availability of such conductors. The recent discovery of high μ and NIR transparent conductors has opened the door to the development of active electronic devices such as fully transparent displays and NIR sensitive solar cells.[2–4,9,10] Since the transparent electronics and visible-NIR sensitive solar cells are in the early stage of development,[11] an understanding of the electrical and optical behavior of the aforementioned transparent conductors must be developed prior to applying them in electronic devices. A high quality TCO of molybdenum doped indium oxide (IMO) thin film was reported by Meng *et al.*[12] Gupta *et al.*[13–16] reported the recent developments on the high mobility indium oxide based TCOs in their studies. IMO thin films have been explored by various deposition techniques such as thermal reactive evaporation,[12] rf magnetron sputtering,[17–19] dc magnetron sputtering,[20] hollow cathode sputtering,[21] pulsed laser ablation,[13,22] and spray pyrolysis.[23–26]

a)Author to whom correspondence should be addressed. Tel.: + 91 431 2407057. FAX: +91 431 2407045. Electronic mail: krmurthin@yahoo.co.in.

Most high quality TCOs are either deposited at a relatively high substrate temperature (T_s) (>450 °C) or deposited on a single crystalline substrate and then annealed at a temperature greater than 500 °C. A high μ of ~130 $cm^2/V\,s$ was reported for evaporated IMO films on In_2O_3 buffer layer (few hundred Å thickness) coated glass substrates at 350 °C with an unintentional vacuum annealing at 300 °C for 5–15 min.[12] Further, μ of ~263 $cm^2/V\,s$ was reported for IMO films deposited using pulsed laser deposition at 500 °C on quartz substrates.[13] IMO films seem to be capable of achieving the unique combination of low ρ and high μ with high NIR transmittance. However, the available reports on these films[12,13] have not studied this aspect in detail. Further, the available reports show that there is inadequate work on these films by employing the conventional and economic spray pyrolysis technique.[23,24] The authors have highlighted this point in their recent short communication.[25] The present study attempts to understand the electrical and optical behaviors of IMO films deposited on Corning-1737 substrates at 400 °C, without postannealing and without any buffer layer, by the spray pyrolysis experimental technique.

II. EXPERIMENTAL

The authors have earlier reported IMO films[26] deposited by the spray pyrolysis technique,[27] where $InCl_3$ was dissolved using methanol as a solvent. Joseph Prince *et al.*[28] demonstrated that indium oxide (IO) films with better properties can be grown at relatively low temperatures (380 °C) by using an ethanol:water mixture as a solvent. Consequently, the films reported in the present study were deposited on Corning-1737 substrates using ethanol:double distilled water (1:3 ratios) as a solvent. The films deposited with T_s in the range of 450–500 °C were opaque with milky white in color[28] and have significantly deteriorated the transmittance. A probable reason is that the pyrolytic decomposition taking place in the hot air layer above the substrate[29] at this T_s range is probably substantiated by the resulting transparent films when the T_s is reduced to 400 °C. Hence, the films reported in this study were all deposited at 400 °C. Further, molybdenum (Mo) doping in the solution was narrowed in between 0 and 1 at. % in order to study the effect of doping content on the physical properties of IMO films in detail. The value of Mo doping (at. %) given in the present work means the ratio of Mo to In in the spray solution. $InCl_3$ and $MoCl_5$ were used as precursors for the source of In and Mo, respectively. The estimated quantity of these precursors was dissolved in ethanol (99.9%) and doubly distilled water. The optimized spray parameters such as the spray nozzle-substrate distance (30 cm), spray angle (~55°), spray time (1 s), spray interval (20 s), and carrier gas pressure (compressed air; 40 kg/cm^2) were kept constant.

X-ray diffraction (XRD) patterns were obtained using the computer controlled PAN Analytic X'Pert PRO XRD system (Cu $K\alpha$ with a wavelength of 1.5406 Å) in the Bragg–Brentano geometry ($\theta/2\theta$ coupled). The electrical parameters were measured at room temperature using a Hall measurement setup (ECOPIA-HMS 3000 Hall system) with a permanent magnet of 0.5 T. The optical transmittance was measured using a double beam spectrophotometer (Shimadzu UV-3100) with a bare substrate in the path of the reference beam. Hence, all the transmittance spectra reported in this study refer only to the film transmittance. The thickness of the films was measured by the reflection method using filmetrics F20, which was in agreement with the values obtained by the weight-gain method. The surface microstructure was examined by field emission scanning electron microscopy (FESEM) (FSI Serion). The composition of different constituents in the deposited films was estimated using energy dispersive x-ray spectroscopy (EDS).

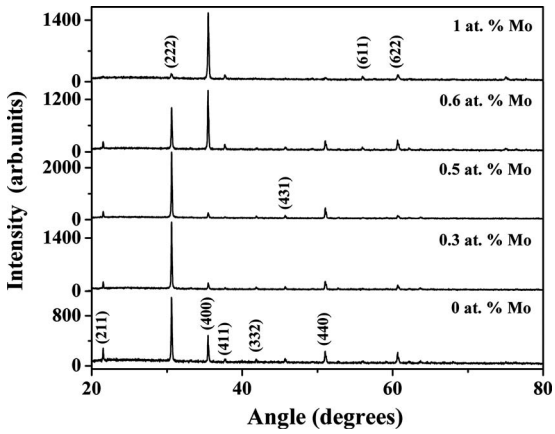

FIG. 1. XRD patterns of IMO thin films with different Mo concentrations.

III. RESULTS AND DISCUSSION

A. XRD

The thickness of all the films was found to be ~300 nm. XRD studies confirmed the cubic bixbyite structure of the polycrystalline In_2O_3 (IO),[30] and the obtained diffraction peaks are identified by matching with the standard data, as shown in Fig. 1. The obtained diffraction peaks substantiate the polycrystalline nature of the IMO films, while their intensities suggest a more uniformly distributed orientation of crystallites. It is perceptible from the figure that the (222) peak emerges as the strongest orientation for the IO films and is retained until 0.5 at. % Mo doping. The increasing intensity of the (222) diffraction peak (I_{222}) with the increase in Mo doping probably suggests the improvement in crystallinity. When the Mo doping is increased further to 0.6 at. %, the intensity of the (400) diffraction peak is significantly increased and tends to emerge as the strongest orientation. This process seems to have been completed when the films are doped with 1 at. % Mo, wherein the (400) peak is emerged as the strongest orientation. For the films doped with 0.6 and 1 at. % of Mo, (I_{222}) considerably decreases whereas the intensity of (400) reflection increases. This change in the strongest orientation due to the variation in Mo doping is also discussed in our earlier work.[26] The foregoing discussion concludes that the intensity of the diffraction peaks can be varied and the strongest orientation can be shifted between the planes by the variation in Mo doping level.

The data extracted from the XRD analysis are summarized in Table I. The full width at half maximum (FWHM)

TABLE I. Data extracted from the XRD analysis as a function of Mo doping (0–1 at. %).

Mo doping (at. %)	Angle 2θ (deg)	*hkl*	I_{222}/I_{400}	Lattice constant (Å)	FWHM (deg)	Crystallite size (nm)
0.0	30.59	(222)	2.74	10.117	0.836	110.4
	35.44	(400)		10.121	0.167	58.3
0.3	30.58	(222)	0.51	10.117	0.836	110.4
	35.44	(400)		10.121	0.067	124.6
0.5	30.60	(222)	14.0	10.111	0.067	138.0
	35.46	(400)		10.116	0.167	35.4
0.6	30.58	(222)	0.70	10.117	0.084	110.4
	35.46	(400)		10.116	0.084	99.7
1.0	30.58	(222)	0.059	10.117	0.200	46.0
	35.49	(400)		10.107	0.100	83.0

value obtained from the (222) and (400) diffraction peaks of IMO thin films increases from 0.0669° to 0.2007° for the various Mo dopings. The crystalline size (L) calculated using Scherrer's formula[31] is varying as a function of Mo doping. The obtained L values corroborate the changes in FWHM due to various Mo doping concentrations. The increase in FWHM suggests that as Mo concentration increases, $L_{(222)}$ decreases while $L_{(400)}$ increases. Moreover, $I_{(222)}$ decreases significantly with increasing Mo concentrations. This behavior indicates that an increase in Mo concentration deteriorates the growth along the (222) plane and improves that along the (400) plane. This could be attributed to the influence of strain arising due to the difference in the ionic radii of molybdenum and indium.[32] The XRD results coupled with FESEM microstructures (Fig. 2) also indicate the reduction in grain size as doping concentration is increased. However, the grain sizes calculated from the FESEM microstructures are larger than the values obtained from the XRD data. Similar results have been observed for aluminum doped ZnO films,[33] where the grain size extracted from the scanning electron microscopy (SEM) microstructures was larger since smaller crystallites were agglomerated together to form larger grains.

The intensity ratio of the $I_{(222)}/I_{(400)}$ is used to evaluate the texture of the deposited IMO thin films. The ratio of the relative intensity of $I_{(222)}/I_{(400)}$ is given in Table I. Values of 2.74, 11.4, and 14 are obtained for the 0.0, 0.3, and 0.5 at. % Mo doped IO films, respectively. This probably indicates a strong crystallographic texture along the [111] direction. Further, for 0.6 and 1 at. % Mo doped IMO thin films $I_{(222)}$ decreases, while that of $I_{(400)}$ increases significantly. Therefore, the corresponding $I_{(222)}/I_{(400)}$ ratio decreases to 0.70 and 0.059, respectively, for 0.6 and 1 at. % Mo doping, thus indicating a strong crystallographic texture change along the [100] direction. The lattice constants (a) calculated from XRD patterns[31] range between 10.107 and 10.121 Å (Table I) and are in agreement with the standard data of the IO film.[30] There is no significant variation in a due to Mo doping, which is presumably due to the fact that the ionic radius of In^{3+} (81 pm) is very close to that of Mo^{6+} (69 pm).

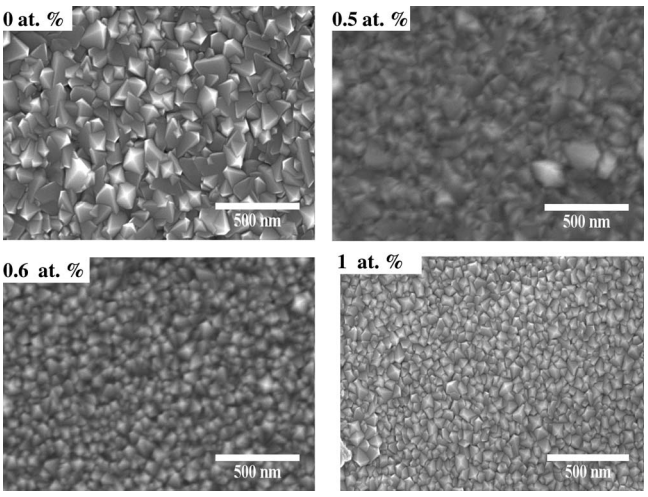

FIG. 2. FESEM images of IMO thin films: 0, 0.5, 0.6, 1 at. % Mo.

B. Scanning electron microscopy

Figure 2 shows the surface microstructures obtained from the FESEM analysis for various Mo doping levels. The IMAGE J software was used to estimate the size of the grains (D) on the surface. The grain sizes (by FESEM) are usually measured by the distance between the visible grain boundaries. In the case of the IO film, the irregularly shaped grains that vary in size between ~60 and ~113 nm are observed together with a few larger grains of ~190 nm. When Mo doping is increased to 0.5 at. %, the grains grow bigger and their sizes range between ~110 and ~160 nm. The grains are irregular in shape but seem to be densely packed. When Mo doping is increased further to 0.6 at. %, the grains become more regular in shape and they are more uniformly distributed over the surface. Further, the size of the grains varies between ~90 and ~135 nm. The shape of the grains is similar to that of the top-angle view of an octahedron and is distinguishable from the shape of grains observed for the films with ≤0.5 at. % Mo doping. The difference in grain shapes probably suggests the difference in the growth orientation, as is evident from the XRD studies. The octahedron shape is retained for the films doped with 1 at. % Mo, and the size of the grains is reduced to values ranging between ~80 and ~100 nm. Overall, the FESEM analysis authenticates that the surface is smooth, fully covered with uniformly distributed grains, and free from pin holes or islands. The deposited films were analyzed by EDS to estimate the actual

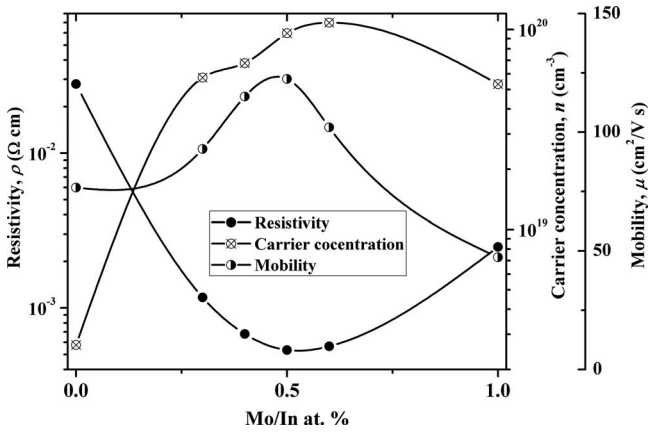

FIG. 3. Variation in electrical properties of IMO thin films as a function of Mo doping.

composition of the constituents. The typical EDS spectra obtained from the films deposited with 0.6 and 1.0 at. % Mo (in the solution) revealed the following data: The at. % of the constituents of Mo, In, and O elements are estimated as 0.31, 40.24, and 59.46 at. % for the films doped with 0.6 at. % Mo, whereas they are estimated as 0.5, 39.55, and 59.95 at. % for the films doped with 1.0 at. % Mo.

C. Hall measurements

The electrical properties are estimated from the room-temperature Hall measurements in the van der Pauw configuration. The negative sign of the Hall coefficient confirmed the *n*-type conductivity. The variation in electrical properties is schematically shown in Fig. 3 as a function of Mo doping levels. The ρ of the IO films is significantly decreased from $\sim 2.8\times10^{-2}$ to $\sim 5.3\times10^{-2}$ Ω cm for the increase in Mo doping from 0.0 to 0.5 at. %. However, ρ is increased for the further increase in Mo doping to reach $\sim 2.4\times10^{-3}$ Ω cm at 1 at. %. On the other hand, the μ of the IO films is extensively increased from ~ 76.6 to ~ 122.4 cm^2/V s for the increase in Mo doping from 0.0 to 0.5 at. % but then decreased thereafter. The probable reason for decreasing μ is the increasing scattering effect due to high impurity. The μ is determined by a few scattering mechanisms. The ionized scattering mechanisms are dominated, and it was discussed in more detail for IMO thin films.[25] The influence of various scattering mechanisms of TCO thin films on the μ of the films was well studied and discussed by various authors.[34–36] A maximum μ of ~ 122.4 cm^2/V s, a low ρ of $\sim 5.3\times10^{-4}$ Ω cm, and *n* of $\sim 9.5\times10^{19}$ cm^{-3} are obtained for the films doped with 0.5 at. % Mo. The obtained results probably indicate that even relatively less Mo has a high doping efficiency in IO, in comparison to the commercial ITO films where the Sn–In ratio is about 10%.[21] Inactive dopants in ITO probably act as scattering centers that reduce the electron mobility. The electrical properties of IMO films obtained from various deposition techniques on glass substrates are summarized in Table II. A higher μ of 130 cm^2/V s was reported by Meng *et al.*[12] for the IMO films deposited at 350 °C by the reactive thermal evaporation method and then by unintentional vacuum annealing at 300 °C for 5–15 min. It is noteworthy that the substrate[12] was coated with few 100 Å of In_2O_3 buffer layer prior to the deposition of IMO films. Gupta *et al.*[13] reported a higher μ with low ρ of IMO thin films at 500 °C on quartz substrates. It can be noticed that in the present work, the highest μ of ~ 122.3 cm^2/V s is obtained for the films deposited on the Corning glass substrate without a postannealing treatment and a buffer layer. It is straightforward that the number of free carriers in the conduction band determines the ρ. Further, it may be noticed that the Mo doping level (0.3–0.5 at. %) in the present study is the lowest among the available reports for which improved electrical properties are obtained. One of the reasons that IMO films acquire high μ is that the relatively small Mo concentration reduces the effect of neutral impurity scattering.[22] Further, the lower *n* extends the *T* further into the NIR region and reduces the magnitude of the free-carrier absorption.[22]

The excess Mo atoms probably do not occupy proper lattice sites in the In_2O_3 crystallites because of their solubility limit. The excess Mo atoms may occupy interstitial positions and deform the crystal structure. The change in preferred orientation from (222) to (400) occurs due to the deformation of the crystal structure when the Mo doping level is increased above 0.5 at. %. The *n* of undoped films (0 at. % Mo) is significantly increased when doped with 0.3 at. % Mo. The increment is gradual until 0.6 at. % Mo but then significantly decreased (1 at. % Mo). The maximum *n* is achieved for 0.5 at. % Mo doping, while 1 at. % Mo doping has the least value. This probably indicates that 1 at. % Mo produces excess Mo atoms that did not occupy proper lattice positions. Further, the higher Mo doping (1 at. %) has probably increased the scattering of ionized impurities, defects, and grain boundaries in the crystal, which in turn reduces the μ and *n*. The behavior of *n* suggests that not all the Mo atoms in the film contribute to donor

TABLE II. Comparison of electrical properties obtained from IMO films (deposited on glass without postannealing) in the present study with other similar reports.

Technique	T_s (°C)	Mo doping	ρ (Ω cm)	n (cm^{-3})	μ (cm^2/V s)	Ref.
Spray pyrolysis	400	0.5 at. %	5.3×10^{-4}	9.5×10^{19}	122.4	This work
Spray pyrolysis	450	1.25 at. %	7.3×10^{-4}	5.0×10^{20}	···	[23]
Spray pyrolysis	400	6 at. %	7.3×10^{-4}	5.0×10^{20}	34.0	[24]
Spray pyrolysis	450	0.5 at. %	1.8×10^{-3}	4.6×10^{19}	77.0	[26]
rf cosputtering	450	3 at. %	1.0×10^{-3}	···	80.0	[37]
rf sputtering	450	4 at. %	···	1.3×10^{20}	83.0	[19]

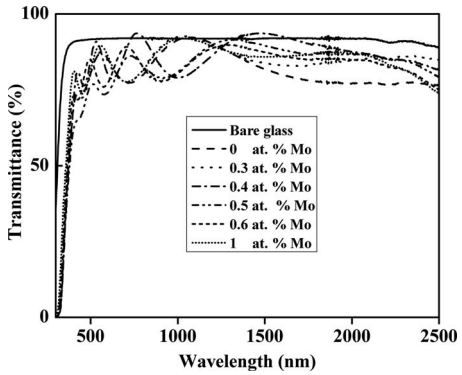

FIG. 4. Optical transmittance spectra of IMO thin films as a function of Mo doping.

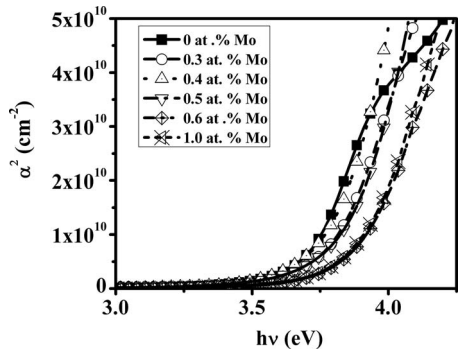

FIG. 5. α^2 vs $h\nu$ plots for IMO thin films with different Mo dopant concentrations.

dopants. When a small amount of Mo impurities ($\leq$0.5 at. %) is added to In_2O_3, they mostly substitute the In existing at lattice sites. This is probably substantiated by the resulting high conducting films at this Mo doping level and suggests 0.5 at. % Mo as the optimal doping level. It is perceptible that n is reduced to $\sim 5.3\times10^{19}$ cm^{-3} when the films are doped with higher Mo doping (1 at. %). This may be due to the fact that the excess Mo atoms result in the intragrain congregation and/or grain-boundary segregation. These excess Mo atoms are electrically inactive, even acting as "electron killers" with the effects such as donor passivation; thus, n are limited.[34] The foregoing discussion indicates that in order to produce high conducting IMO films, it is necessary to deliberately optimize the amount of Mo in In_2O_3. Further, it is concluded that ρ of the IMO film is related to the Mo doping concentration, intrinsic defects (e.g., Mo interstitials and O vacancies), and various scattering centers.

D. Optical properties

The transmittance spectra recorded in the wavelength range of 300–2500 nm are shown in Fig. 4 as a function of the Mo doping level. The average transmittance (AT) is $\sim$83% in the wavelength ranging 400–2500 nm. The data extracted from the transmittance spectra are quantified in Table III. The maximum average visible transmittance (AVT) is $\sim$93.6% at 766 nm for the films doped with 0.4 at. % Mo, whereas a minimum AVT of $\sim$74% at 576 nm is obtained for 0.3 at. % Mo. In the NIR range, all the films exhibit $T > 83\%$ at around 1500 nm and close to 80% at around 2500 nm. For all the IMO films, the AT in the blue region is $\sim$70% in the wavelength range of 400–500 nm. A maximum AT of 85% in the blue region (496 nm) is obtained for the films doped with 0.4 at. % Mo, whereas a minimum AVT of 61% in the blue region (400 nm) is obtained for those deposited with 0.5 at. % Mo. The obtained values suggest that the IMO films could be useful for the applications where higher NIR transmittance is required. This high NIR transmittance is also observed in undoped SnO_2 (Ref. 38) and IO (Ref. 39) films having similar carrier concentrations but with considerably high ρ. In contrast, the transmittance of the ITO films is decreased in the NIR region (>1000 nm) due to the high degree of free-carrier absorption. The IMO thin films deposited in the present study do not observe plasma frequency in the wavelength range up to 2500 nm. It is perceptible from Fig. 4 that the transmission window of the IMO films is significantly larger than that of the ITO films.[39] This means the degree of free-carrier absorption is significantly reduced in IMO films presumably due to the high μ. The high n of 1.0×10^{20} cm^{-3} obtained for the films doped with 0.6 at. % Mo, in the present study, is one order of magnitude lower than the typical polycrystalline ITO thin films.[40] From the plot of absorption coefficient $(\alpha)^2$ (V s) photon energy $(h\nu)$ (Fig. 5), the optical band gap (E_g) of the films was estimated.[41] A minimum value of 3.65 eV obtained for the IO films is increased to a range of 3.78–3.93 eV for various Mo doping levels. Theoretically, a gap of at least 3.5 eV[5] is needed for a TCO in most anticipated applications, and the films prepared in this study have achieved this requirement. This increase in E_g can be related to the shifting of the absorption edge toward the near UV range. The increase in E_g with the increasing n can be explained on the basis of the Burstein–Moss (BM) effect,[42] an energy band widening ef-

TABLE III. Optical data obtained from the deposited IMO films as a function of Mo doping levels.

Mo doping (at. %)	AVT (500–800 nm) (%)	Band gap (eV)	Figure of merit (Ω^{-1})	NIR transparent at different wavelengths		
				1500 nm	2000 nm	2500 nm
0.0	81.3	3.65	2.0×10^{-3}	82.7	79.3	78.8
0.3	87.4	3.78	5.0×10^{-3}	83.8	84.7	84.7
0.4	84.6	3.80	5.2×10^{-3}	93.5	87.5	81.5
0.5	77.0	3.88	4.0×10^{-2}	89.5	86.6	78.9
0.6	81.6	3.89	8.1×10^{-2}	87.3	84.7	75.0
1.0	82.3	3.93	2.6×10^{-3}	85.8	87.0	73.6

fect resulting from the increase in the Fermi levels in the conduction band of degenerated semiconductors. Assuming that the conduction band and valence band are parabolic in nature and that the BM shift is the predominant effect, we can write

$$E_g = E_{g0} + \Delta E_g^{B-M}, \tag{1}$$

where E_{g0} is the intrinsic band gap and ΔE_g^{B-M} is the BM shift due to the filling of low lying levels in the conduction band.[42] An expression for the BM shift is given by

$$\Delta E_g^{B-M} = (h^2/8\pi^2 m_{vc}^*)(3\pi^2 n)^{2/3}, \tag{2}$$

where n is the carrier concentration and m_{vc}^* is the reduced effective mass of the carriers. From this expression, it is clear that the BM shift is directly proportional to $n^{2/3}$. However, at very high n, it is seen that there is a band gap narrowing due to electron-electron scattering and electron-impurity scattering.[43,44] It can be noticed that the variation trend of E_g is in good agreement with that of n. The figure of merit (Φ) (Ref. 45) for a transparent conductor for photovoltaic applications is given by

$$T_a^{10}/R_s, \tag{3}$$

where T_a is the AT in the visible range and R_s is the sheet resistance of the film, and the estimated Φ values are given in Table III. The highest value for $(\Phi) = 4.07 \times 10^{-2}\ \Omega^{-1}$ was observed for the 0.5 at. % IMO thin film.

IV. CONCLUSION

IMO thin films with high carrier mobility and high NIR transparency are deposited on Corning-1737 glass substrates by the spray pyrolysis experimental technique. The films have been studied in detail as a function of the content of Mo ranging from 0 to 1 at. %. The XRD studies confirmed polycrystalline films having a cubic bixbyite structure (space group 206) with no evidence of Mo or MoO_3. A low resistivity of $\sim 5.3 \times 10^{-4}\ \Omega$ cm, a carrier concentration of $\sim 9.5 \times 10^{19}\ \mathrm{cm}^{-3}$, a high carrier mobility of $\sim 122.4\ \mathrm{cm}^{-2}/\mathrm{V\,s}$, and a figure of merit of $4.07 \times 10^{-2}\ \Omega^{-1}$ were obtained for the films doped with 0.5 at. % Mo. The AVT (500–800 nm) is higher than 80%, and the transmittance is well extended into the NIR region. The obtained wide spectral range of transmittance suggests that the deposited IMO films could be utilized in the optoelectronic devices where high NIR transmittance is demanded. The morphological studies confirmed the well packed grains with a smooth surface. The obtained results suggest that the IMO films can be developed as an ITO-alternative material in various applications such as thin film transistors and NIR sensitive solar cells.

ACKNOWLEDGMENTS

S.P. and K.R. thank the Inter University Accelerator Center, New Delhi, India for providing the financial support through the UFUP Project scheme (Project No. UFUP-41313). S.P. thanks the Council of Scientific Industrial and Research, New Delhi, India for offering Senior Research Fellowship. E.E. thanks the Portuguese Ministry of Science and Technology (FCT-MCTES) for offering the postdoctoral fellowship (Ref. No. SFRH/BPD/35055/2007). This work is partially funded by FCT-MCTES through CENIMAT/I3N, FCT-UNL, Portugal

[1] T. Koida and M. Kondo, Appl. Phys. Lett. **89**, 082104 (2006).
[2] K. Nomura, H. Ohta, A. Takagi, T. Kamiya, M. Hirano, and H. Hosono, Nature (London) **432**, 488 (2004).
[3] E. Fortunato, P. Barquinha, A. Pimentel, G. Gonçalves, A. Marques, L. Pereira, and R. Martins, Adv. Mater. **17**, 590 (2005).
[4] T. Koida, H. Fujiwara, and M. Kondo, Appl. Phys. Express. **1**, 041501 (2008).
[5] T. J. Coutts, D. L. Young, and X. Li, MRS Bull. **25**, 58 (2000).
[6] J. A. Anna Selvan, A. E. Delahoy, S. Guo, and Y.-M. Li, Sol. Energy Mater. Sol. Cells **90**, 3371 (2006).
[7] G. Frank and H. Köstlin, Appl. Phys. A: Mater. Sci. Process. **27**, 197 (1982).
[8] E. Fortunato, D. Ginley, H. Hosono and, D. C. Paine, MRS Bull. **32**, 242 (2007).
[9] J. W. Bowers, H. M. Upadhyaya, S. Calnan, R. Hahimoto, T. Nakada, and A. N. Tiwari, Prog. Photovoltaics **17**, 265 (2009).
[10] S. Calnan, H. M. Uphadhyaya, S. Buecheler, G. Khrypunov, A. Chirila, A. Romeo, R. Hashimoto, T. Nakada, and A. N. Tiwari, Thin Solid Films **517**, 2340 (2009).
[11] E. Fortunato, L. Raniero, L. Silva, A. Goncalves, A. Pimentel, P. Barquinha, H. Aguas, L. Pereira, G. Goncalves, I. Ferreira, E. Elangovan, and R. Martins, Sol. Energy Mater. Sol. Cells **92**, 1605 (2008).
[12] Y. Meng, X. L. Yang, H. Chen, J. Shen, Y. M. Jiang, Z. J. Zhang, and Z. Y. Hua, Thin Solid Films **394**, 218 (2001).
[13] R. K. Gupta, K. Ghosh, R. Patel, and P. K. Kahol, Appl. Surf. Sci. **255**, 3046 (2008).
[14] R. K. Gupta, K. Ghosh, S. R. Mishra, and P. K. Kahol, Appl. Surf. Sci. **254**, 1661 (2008).
[15] R. K. Gupta, K. Ghosh, S. R. Mishra, and P. K. Kahol, Thin Solid Films **516**, 3204 (2008).
[16] R. K. Gupta, K. Ghosh, and S. R. Mishra, Mater. Lett. **62**, 1033 (2008).
[17] E. Elangovan, G. Goncalves, R. Martins, and E. Fortunato, Sol. Energy **83**, 726 (2009).
[18] Y. Yoshida, T. A. Gessert, C. L. Perkins, and T. J. Coutts, J. Vac. Sci. Technol. A **21**, 1092 (2003).
[19] Y. Yoshida, D. M. Wood, T. A. Gessert, and T. J. Coutts, Appl. Phys. Lett. **84**, 2097 (2004).
[20] X. Li, W. Miao, Q. Zhang, L. Huang, Z. Zhang, and Z. Hua, J. Mater. Res. **20**, 1404 (2005).
[21] A. E. Delahoy and S. Y. Guo, J. Vac. Sci. Technol. A **23**, 1215 (2005).
[22] C. Warmsingh, Y. Yoshida, D. W. Readey, C. W. Teplin, J. D. Perkins, P. A. Parilla, L. M. Gedvilas, B. M. Keyes, and D. S. Ginley, J. Appl. Phys. **95**, 3831 (2004).
[23] D. J. Seo and S. H. Park, Physica B **357**, 420 (2004).
[24] P. Prathap, G. Gowri Devi, Y. P. V. Subbaiah, V. Ganesan, K. T. Ramakrishna Reddy, and J. Yi, Phys. Status Solidi A **205**, 1947 (2008).
[25] S. Parthiban, K. Ramamurthi, E. Elangovan, R. Martins, and E. Fortunato, Appl. Phys. Lett. **94**, 212101 (2009).
[26] S. Parthiban, V. Gokulakrishnan, K. Ramamurthi, E. Elangovan, R. Martins, E. Fortunato, and R. Ganesan, Sol. Energy Mater. Sol. Cells **93**, 92 (2009).
[27] E. Elangovan, K. Ramamurthi, and J. Optoelectron, Adv. Mater. **5**, 45 (2003).
[28] J. J. Prince, S. Ramamurthy, B. Subramanian, C. Sanjeeviraja, and M. Jayachandran, J. Cryst. Growth **240**, 142 (2002).
[29] H. L. Hartnagell, A. L. Dawar, A. K. Jain, and C. Jagadish, *Semiconducting Transparent Thin Films* (IOP, London, 1995).
[30] Powder Diffraction (JCPDS)–International Centre for Diffraction Data (ICDD) Card No. 06-0416, Philadelphia, PA, 2005.
[31] B. D. Cullity, *Elements of X-Ray Diffraction* (Addison-Wesley, Reading, MA, 1956).
[32] J. Nishino, S. Ohshio, and K. Kamata, J. Am. Ceram. Soc. **75**, 3469 (1992).
[33] S. Mridha and D. Basak, J. Phys. D: Appl. Phys. **40**, 6902 (2007).
[34] J. G. Lu, Z. Z. Ye, Y. J. Zeng, L. P. Zhu, L. Wang, J. Yuan, B. H. Zhao, and Q. L. Liang, J. Appl. Phys. **100**, 073714 (2006).
[35] R. B. Dingle, Philos. Mag. **46**, 831 (1955).
[36] T. Koida and M. Kondo, J. Appl. Phys. **99**, 123703 (2006); **101**, 063713

(2007).
[37]N. Yamada, T. Tatejima, H. Ishizaki, and T. Nakada, Jpn. J. Appl. Phys., Part 2 **45**, L1179 (2006).
[38]E. Shanthi, V. Dutta, A. Banerjee, and K. L. Chopra, J. Appl. Phys. **51**, 6243 (1980).
[39]C. E. Wickersham and J. E. Greene, Phys. Status Solidi A **47**, 329 (1978).
[40]H. Ohta, M. Orita, M. Hirano, H. Tanji, H. Kawazoe, and H. Hosono, Appl. Phys. Lett. **76**, 2740 (2000).
[41]I. Hamberg and C. G. Granqvist, J. Appl. Phys. **60**, R123 (1986).
[42]E. Burstein, Phys. Rev. **93**, 632 (1954).
[43]P. A. Wolff, Phys. Rev. **126**, 405 (1962).
[44]K. F. Berggren and B. E. Sernelius, Phys. Rev. B **24**, 1971 (1981).
[45]G. Haacke, J. Appl. Phys. **47**, 4086 (1976).